

pubs.acs.org/cm Article

Role of Secondary Thermal Relaxations in Conjugated Polymer Film Toughness

Nrup Balar, Salma Siddika, Somayeh Kashani, Zhengxing Peng, Jeromy James Rech, Long Ye, Wei You, Harald Ade, and Brendan T. O'Connor*



Cite This: https://dx.doi.org/10.1021/acs.chemmater.0c01910



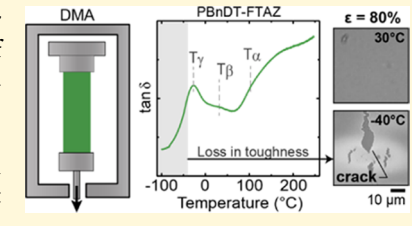
ACCESS

III Metrics & More

Article Recommendations

Supporting Information

ABSTRACT: Conjugated polymers have proven to be an important class of materials for flexible and stretchable electronics. To ensure long-term thermal and mechanical stability of associated devices, there is a need to determine the origin of the polymer ductility and toughness. In this work, we investigate a variety of high-performance conjugated polymers and relate their thermomechanical behavior to film toughness. Dynamic mechanical analysis (DMA) is used to probe thermomechanical relaxations of the conjugated polymers. Film ductility is measured as a function of temperature to determine the temperature that corresponds to a significant loss in film toughness. We systematically study polymers with



changes to the side-chain structure, backbone structure, and crystallinity. We also compare polymers that have a clear glass transition $(T_{\rm g})$ to those that do not. It is found that secondary thermal relaxations (sub- $T_{\rm g}$) play a critical role in film toughness. This sub- $T_{\rm g}$ is found to be a local molecular relaxation that appears to relate to side-chain and backbone mobility. We also find that many of the polymers considered continue to show moderate ductility below their sub- $T_{\rm g}$, which is attributed to crystallites or aggregates that have active slip systems. These results provide new insights into how conjugated polymer structure and related thermal relaxations influence film toughness that will assist in realizing mechanically robust devices.

1. INTRODUCTION

Organic electronics continue to be of substantial research interest owing to their ability to achieve unique capabilities including flexible and stretchable devices for medical, 1,2 display,^{3,4} power generation,^{5,6} and numerous other applications.^{7–9} During device processing and operation, these power generation,^{5,6} and numerous other applicadevices undergo mechanical and thermal loads that can affect both their lifetime and performance. Thus, to ensure reliable operation, it is imperative that the underlying properties of the materials that impact performance and reliability are accurately captured. While conjugated polymers (CPs) can have favorable attributes that lend themselves to mechanically robust operation, their mechanical response is strongly dependent on their thermal state. Recently, in an effort to increase ductility and toughness, CPs have been synthesized with glass transitions $(T_{\sigma}s)$ below room temperature (RT). However, polymers with significant viscoelastic relaxation behavior can be undesirable due to their propensity for morphological changes over time that can lead to deterioration in device performance. 14,15 This is particularly true in blend films that are not in thermodynamic equilibrium. 16,17 A similar challenge is faced in polymers for structural applications that are required to be stiff, thermally stable, and tough. The combination of stiff and tough can be achieved in some polymers with the classic example being polycarbonate (PC), which is tough at room temperature but has a $T_{\rm g}$ > 100 °C providing stiffness. ^{18,19} This behavior has been ascribed to secondary thermomechanical relaxations that occur below its

 $T_{\rm g}$. The origin of secondary relaxations is typically attributed to molecular motion in side-chains 10 or localized motion in the backbone. ²¹ It is at the sub- T_g transition where many polymers transition from ductile and tough to brittle and weak as the temperature is decreased, which is identified as the ductile-tobrittle transition temperature. 10 However, as opposed to many commodity polymers such as PC, many recently developed CPs do not show a clear T_g . In addition, they differ structurally in significant ways, including having flexible aliphatic sidechains and rigid conjugated ring structures along the backbone. Thus, we are interested in determining the structural origin to the thermomechanical relaxation in CPs and how this impacts film toughness. Capturing the origin of the thermal relaxations and their impacts on mechanical behavior will facilitate design strategies to achieve mechanically robust, morphologically stable, and high-performance devices.

In this report, the thermomechanical relaxation behavior in a representative set of high-performance CPs (Figure 1) was characterized using a dynamic mechanical analyzer (DMA). We then compared the thermal relaxation behavior to changes in film toughness. The film toughness was probed by

Received: May 5, 2020 Revised: July 7, 2020 Published: July 8, 2020



Figure 1. Molecular structures of the polymers studied.

measuring differences in crack behavior of films strained on elastomer substrates at different temperatures. We first introduce our experimental approach using poly(methyl methacrylate) (PMMA) as a model system that clearly shows a ductile-to-brittle transition associated with its thermal relaxations. The CPs considered have systematic structural differences to isolate the role of various moieties on film toughness. We consider polymers that show a clear T_{σ} and those that do not, polymers with differences in crystallinity, and polymers with systematic variation in the backbone and side-chain structures. We find that across all CPs considered, the secondary thermal relaxations (sub- T_g s) play a significant role in the toughness of the films. In most of the polymers considered, a significant drop in toughness coincided closely with the peak in the loss modulus associated with the sub- $T_{\rm g}$. While the secondary transitions appear to be localized noncooperative relaxations that exhibit Arrhenius behavior, there are signatures in several polymers that suggest that the transition involves relaxation of the side-chains and backbone.

Interestingly, the loss in toughness in the majority of conjugated polymers considered is not as abrupt as observed in many commodity polymers and as we found for PMMA. Below their sub- T_g s, the CPs continue to dissipate energy that arrests crack propagation. This is attributed to crystallites or aggregates, which can support polymer deformation through active slip systems.²² To gain insight into the mechanical behavior, we also performed density functional theory simulations to estimate the persistence length of the polymers considered.²³ We did not find a strong correlation between backbone stiffness and the ductile-to-brittle transition temperature or the characteristics of crack formation and propagation. This is attributed to the dominance of the side-chains on the mechanical behavior of the films. Based on these results, insights into the role of the polymer structure and thermal transitions on mechanical behavior are discussed.

2. EXPERIMENTAL SECTION

2.1. Materials. Eight CPs with different molecular structures were chosen for the study, as shown in Figure 1. High-molecular-weight variants of these polymers were chosen so that the toughness of the polymer films is not limited by lack of entanglements and the role of thermal transitions could be explicitly probed. The molecular weight (MW) and dispersity (D) of the selected polymers are provided in Table 1. Regiorandom (RRa) and regioregular (RR) variants of P3HT were purchased from Rieke Metals. The RR P3HT had a regioregularity of 91–94%. P(NDI2OD-T2), DPP-DTT, and DPP4T were procured from Ossila. PCDTBT was supplied by Sigma-Aldrich and PTB7-TH was supplied by Solarmer. PBnDT-FTAZ²⁵ and PBoDT-FTAZ²⁶ were synthesized as previously reported. PMMA with weight averaged molecular weight ($M_{\rm w}$) of \sim 120 kg/mol was purchased from Sigma-Aldrich.

2.2. Thermal Relaxation Measurements. The thermomechanical behavior of the polymers was characterized using a TA Instruments DMA 850. The polymers were drop cast onto a woven glass mesh that could then be loaded into the DMA following a procedure described in detail elsewhere.^{24,27} Here, we drop cast solutions onto the mesh using the same solvent used to cast films, given in Table S1. The thermal transitions of the polymers were obtained by running temperature scans at an oscillation frequency of 1 Hz and an oscillating strain of 0.1% in tensile mode, illustrated in Figure 2a. The temperature ramp of 3 °C/min was used, and the peaks in the $\tan\delta$ curve were used to identify thermal transition temperatures. Prior to running the scans, the samples were heated to 100 °C to remove any residual solvent and moisture and then rapidly cooled to -110 °C at the rate ~ 30 °C/min. Further, DMA scans were performed at frequencies ranging from 0.5 to 10 Hz to create transition maps and calculate activation energies.

Table 1. Details of the Polymers Considered Including Molecular Weights (MWs), Dispersity (D), Measured Crack Onset Strain (COS) at RT (COS_{RT}), and Thermal Transition Temperatures

polymer	$M_{ m w}$ (kg/mol)	Đ	COS _{RT} (%)	T_{α} (°C)	T_{β} (°C)	T_{γ} (°C)	$T_{b'}$ (°C)
PMMA	120	NA	<3	126	20 ^a		40
RR P3HT	54	2.4	80	25	-78^{a}		-110
RRa P3HT	72	2.97	>100	28	$-79^{a,b}$		-90
PCDTBT	120	NA	30	140	6 ^a		50
PTB7-TH	129	2.01	80	113 ^b	-2^a		0
P(NDI2OD-T2)	168	1.82	60	120 ^b	-21^{a}		-40
PBnDT-FTAZ	223	1.91	>100	119 ^b	30	-26^{a}	-40
PBoDT-FTAZ	164	3.5	>100	55	21 ^b	-39^{a}	-40
DPP4T	171	2.45	90	129 ^b	6 ^a	-52^{b}	-20
DPP-DTT	292	3.9	33	129 ^b	2 ^a	-53 ^b	-50

^aDefined as $\{T_{\beta}\}$. ^bIdentified from the loss modulus peak. ^cNA: not available

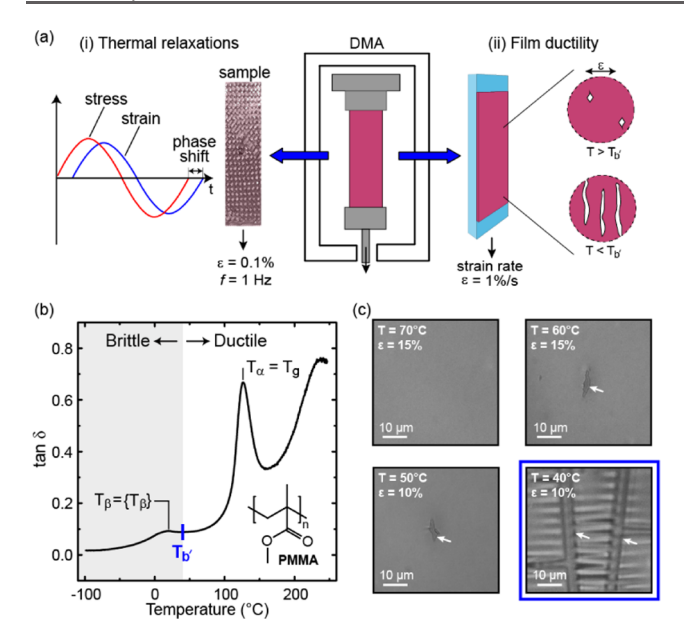


Figure 2. (a) Illustration of the experimental procedure that uses a dynamic mechanical analyzer to determine (i) the thermal relaxation of the polymer films through DMA temperature sweeps and (ii) the ductility of the films by monitoring film fracture under tensile strain. (b) DMA thermogram of PMMA and (c) optical microscope images of PMMA films at a specified strain. The films were strained at the temperature given in the images and strains were along the horizontal axis of the page.

2.3. Ductility Measurements. To measure the film ductility as a function of temperature, the films were placed on thin polydimethylsiloxane (PDMS) elastomer substrates (SLYGARD 184) and strained in tension in the DMA. The samples were prepared by first spin coating poly(4-styrenesulfonic acid) (PSS, Sigma-Aldrich) solution on clean glass substrates at 5000 rpm for 30 s followed by annealing at 150 °C for 5 min. The PSS solution consisted of 1% by weight of PSS in deionized water. Subsequently, the conjugated polymer solutions were spin-coated following the recipes given in Table S1. The thin PDMS support film was prepared by mixing the elastomer base with the curing agent at a weight ratio of 15:1. Prior to curing, the PDMS was spin-coated on a PSS-coated glass substrate at 4000 rpm for 2 min and annealed for 2 h at 150 °C, resulting in ~10 μ m thick films. Once the films were prepared, we transfer-print the films to a thick PDMS slab sequentially and then remove the CP/thin PDMS composite from the thick PMDS slab to obtain the specimen for testing, as illustrated and discussed in detail by Song et al. 28 More specifically, the thin PDMS on PSS-coated glass was laminated to the thick PDMS support (base to curing agent ratio of 5:1). This composite was then placed in water to dissolve the underlying PSS and remove the glass substrate. The CP film was then transferred onto the thin PDMS film by again laminating the film onto the PDMS and immersing the sample in water to remove the PSS and detach the substrate. The CP/thin PDMS composite was then removed from the thick PDMS slab and loaded into the DMA. The DMA is equipped with a furnace that allows fine control of the sample temperature. The PDMS also has a large rubbery plateau with a glass transition near −125 °C and an upper working temperature of over 200 °C, allowing the ductility to be probed over all measured thermal transitions found in the CPs.²⁹ The composite specimens were strained to a prescribed strain at the strain rate of 1%/s. The strained sample was brought back to RT and removed from the DMA and clamped onto a glass slide. The sample was then observed under an optical microscope to determine the crack formation and crack characteristics. The test method is schematically shown in Figure 2a. When heating (cooling) the sample, the PDMS expansion may result in a small tensile (compressive) strain on the CP film; however, the resulting strain is

expected to be much lower than the strain applied to measure crack behavior and is neglected. The films were also strained directly on a custom strain stage while under an optical microscope to determine the crack onset strain at RT.

3. RESULTS AND DISCUSSION

3.1. Approach. Throughout the article, thermal transitions are identified from peaks in the $\tan \delta$ curve unless otherwise specified. The highest temperature peak is identified as T_{α} followed by T_{β} and T_{γ} in order of descending temperature. In polymers that exhibit a clear glass transition, T_{α} is also referred to as $T_{g\gamma}$ while in polymers where we observe a relaxation we attribute to aggregates, T_{α} is referred to as $T_{\alpha,\alpha}$. The strongest secondary transition is referred to as $\{T_{\beta}\}$, which may be the T_{β} or T_{γ} peak, depending on the polymer considered. $T_{b\gamma}$ is identified as the temperature associated with a significant loss in toughness described further below.

We start by demonstrating the approach used to study the thermomechanical behavior of the polymers by considering the well-characterized commodity polymer PMMA. A clear ductile-to-brittle transition temperature in PMMA has been previously reported that is associated with the polymer's secondary thermal relaxation $(T_{\beta})^{20}$ This transition has been attributed to the twisting motion of the methacrylate (-COOCH₃) group. ²⁰ Here, we measure the thermal transitions of PMMA using the glass mesh approach, with $\tan \delta$ shown in Figure 2b. The storage and loss modulus are given in Figure S11. We observe a T_{α} (or T_{g}) at 126 °C and T_{β} $(=\{T_{\beta}\})$ at 20 °C. These observed transitions are within the range of reported values found in the literature. 20,30 Differences in reported values can be due to variations between polymers such as MW and tacticity as well as casting conditions.³¹ The test method and associated kinetics being probed may also differ.

The ductile-to-brittle transition in polymers can be identified by observing the transition of fracture under tensile loading from failure that occurs after yielding (ductile) to failure that occurs prior to significant yielding (brittle). This transition represents a large drop in toughness, which is the area under the stress-strain curve loaded to sample failure. Given that we are dealing with thin films, conventional tensile tests that can capture the full stress-strain behavior are difficult to implement, particularly with fine control of the sample temperature.^{32,33} Thus, we probe the loss in toughness by measuring the film's fracture behavior when strained on an elastomer substrate. We have previously demonstrated that measuring the crack onset strain (COS) using the film on elastomer (FOE) approach is correlated with the film's fracture toughness.³⁴ In addition, Alkhadra et al. have demonstrated that the crack features in a FOE test can be used to characterize the toughness of a polymer film.³⁵ However, it is known that the adhesion and modulus mismatch between a substrate and thin film can have a large influence in the fracture characteristics of the thin film including the COS. 35,36 For example, the elastomer support will increase the COS relative to a free-standing film.²⁸ In addition, the FOE sample is strained while inside a furnace that enables precise temperature control, but limits the ability to determine the COS at a given temperature. Given these constraints, we probe changes in film toughness by monitoring changes in the film's fracture characteristics when strained to a set value. We do this by first determining the COS of the film at room temperature (COS_{RT}) . If the film is brittle at RT, it is heated to a point

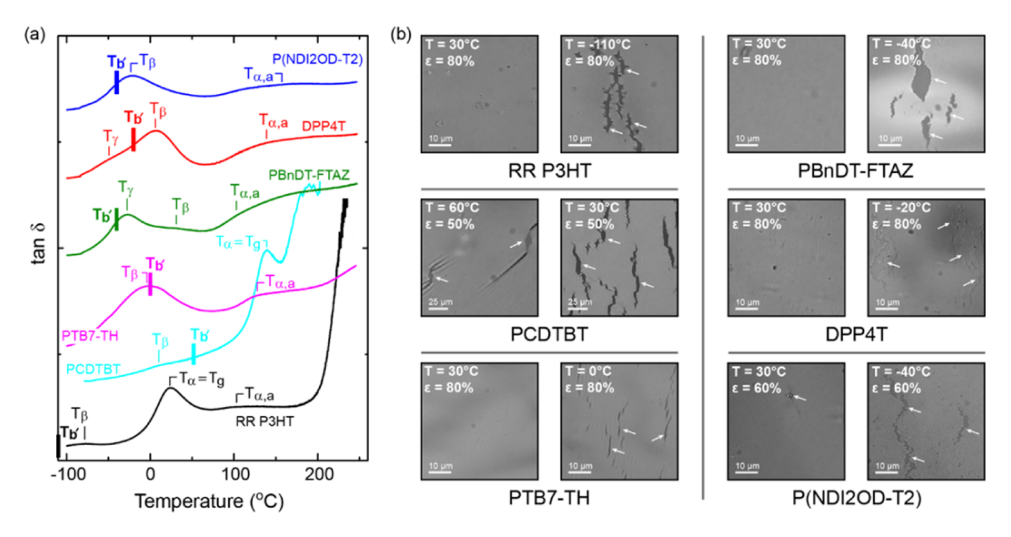


Figure 3. (a) Tan δ curves of different polymers obtained from DMA temperature sweeps. T_{ar} T_{jr} represent observed thermal relaxations, $T_{b'}$ is the measured loss in toughness. $T_{a,a}$ in PTB7-TH, DPP4T, and PBnDT-FTAZ was determined from the peak in loss modulus. (b) Images of the polymer films, including RR P3HT, PCDTBT, PTB7-TH, PBnDT-FTAZ, DPP4T, and P(NDI2OD-T2) at 30 °C and respective $T_{b'}$ stretched to the specified strains. The films were strained along the horizontal axis of the page.

where it is found to be ductile. We then consistently strain the samples to near the measured ductile COS while varying the temperature of the samples. The temperature is reduced in increments of 10 °C, and the temperature where we observe a significant loss in ductility is defined as $T_{\rm b'}$. Here, we use $T_{\rm b'}$ as opposed to the ductile-to-brittle transition temperature ($T_{\rm b}$) as we are probing the temperature of significant toughness loss, but not necessarily a transition to brittle behavior as discussed below.

PMMA is brittle at room temperature (COS_{RT} < 3%), and thus, we started by heating the sample to 70 °C and straining the film by 30%. Very small cracks were observed in the PMMA film when strained to 30% (Figure S1). If we reduced the strain to 15%, no cracks were found (Figure 2c), and thus, we use 15% strain to probe the ductile-to-brittle transition. As the temperature of the PMMA/PDMS composite is decreased to 50 °C, cracks are observed at 15% strain that self-arrest and are pyramidal in shape, which is characteristic of ductile fracture. When decreasing the sample temperature to 40 °C, there is an abrupt change in crack features, which become channel-like, indicating a transition from ductile-to-brittle behavior, as shown in Figure 2c. 34,35 From these observations, we identify $T_{b'}$ for PMMA to be approximately 40 °C. This transition temperature matches similar measurements of the ductile-to-brittle transition in bulk PMMA samples.³⁷ The similar ductile-to-brittle transition found between the methods demonstrates the efficacy of this approach. Here, we find that $T_{\rm b'}$ is roughly 20 °C higher than T_{β} , similar to previous reports. Details of the relationship between thermal relaxations in PMMA and sample ductility are discussed further elsewhere.²⁰

3.2. Polymers With a Clear $T_{\rm g}$. The first CPs considered are RR P3HT and PCDTBT that show a clear glass transition. The DMA scans for these polymers are provided in Figures 3 and S12. These measurements reveal RR P3HT to have a $T_{\rm g}$ of 25 °C and a seconadary transition $\{T_{\beta}\}$ at approximately -80 °C. This is consistent with other measurements of high MW RR P3HT using DMA or shear rheology. At RT (30 °C), the RR P3HT films are ductile with a COS measured to be slightly greater than 80%. Thus, following the protocol outlined above, we strain the RR P3HT films to 80% while

holding the sample at a given temperature. As we reduce the temperature of the samples below RR P3HT's T_g , no cracks are observed in the films, and thus, there was no observable change in ductility. Crack formation begins to appear as the sample is cooled to $-30\,^{\circ}$ C, as shown in Figure S2. These crack features are pyramidal in nature consistent with the ductile films where cracks initiate near defects and are quickly arrested. The appearance of cracks is indicative of some loss in toughness, but the large strain and arrested nature suggest that the loss in toughness is minor. It was only when the sample was cooled to $-110\,^{\circ}$ C that the formation of large almost channel-like cracks were observed, as shown in Figure 3, which we identify as T_b . This change in mechanical behavior is near $\{T_{\beta}\}$ ($-80\,^{\circ}$ C), which has been shown to be associated with the relaxation of the alkyl side-chains. 15,38,39 Thus, the change in ductility at $-110\,^{\circ}$ C is attributed to kinetically frozen side-chains.

The PCDTBT DMA results are provided in Figures 3a and S12, exhibiting a T_g = 140 °C and $\{T_\beta\}$ = 6 °C. At RT, the COS was measured to be approximately 30%. While this is relatively large, tensile tests of pseudo-free-standing films using a film-on-water (FOW) test method shows that there is very little yielding prior to film fracture, as shown in Figure S15 (see the Supporting Information (SI) for details). This suggests that PCDTBT is brittle at RT. Yet, at RT, the film is above $\{T_{\beta}\}$, which we attribute to the relaxation of the branched side chains. To probe the effect of $\{T_{\beta}\}$ on film ductility, the sample temperature was reduced down to −30 °C, but no change in crack features was observed, as shown in Figure S3. In contrast, when the sample temperature was increased, we observed that the film ductility increased significantly when the sample was held above 50 °C. At 60 °C, small pyramid-shaped cracks are only found when the sample is strain by 50%, as shown in Figure 3. Thus, we estimate $T_{b'}$ of PCDTBT to be approximately 50 °C. This drop in toughness lies between T_g and $\{T_{\beta}\}$. Interestingly, when the DMA temperature scans were run at an oscillation frequency of 10 Hz, a thermal relaxation at 67 °C became visible, as shown in Figure S14. PCDTBT has been reported to have a unique molecular packing motif with bilayer backbone ordering that may lead to the unique relaxation observed at 10 Hz.40 While this

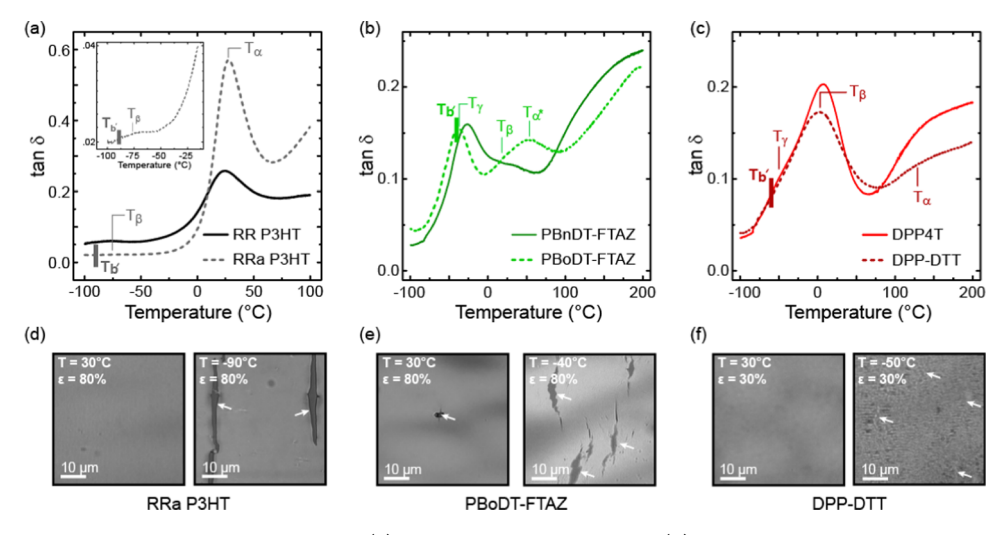


Figure 4. Tan δ curves obtained from the DMA scans of (a) RR P3HT and RRa P3HT, (b) PBnDT-FTAZ and PBoDT-FTAZ, and (c) DPP4T and DPP-DTT. The inset in (a) shows the log(tan δ) vs T of RRa P3HT for better clarity of the β transition in RRa P3HT. (d–f) Optical micrographs of the cracks observed for different polymers at specified temperatures and strains. The films were strained along the horizontal axis of the page.

transition is weak and buried in the DMA scan at 1 Hz, it likely plays an important role in PCDTBT ductility.

3.3. Polymers Without a Clear T_{q}. Many of the recently developed donor-acceptor copolymers do not show a clear glass transition as measured in differential scanning calorimetry (DSC) or DMA.41-43 These polymers mainly comprise of electron-donating and electron-accepting groups along the backbone that can increase the backbone stiffness. 44,45 The stiff polymer chains often require large aliphatic side-chain groups to ensure solubility. Here, we consider several of these polymers with this characteristic lack of glass transition, including PTB7-TH, PBnDT-FTAZ, DPP4T, and P-(NDI2OD-T2). DSC measurements of these polymers are provided in Figure S18, where no T_{σ} could be observed. The DMA scans of these polymers are provided in Figures 3a and S12. For each polymer, we observe a broad thermal transition between 100 and 160 °C, labeled $T_{\alpha,a}$. Note that in PTB7-TH, P(NDI2OD-T2), PBnDT-FTAZ, and DPP4T, the peak in the loss modulus was used to define $T_{\alpha,a}$ given the broad shoulder observed in tan δ . Thermal transitions with similar features have been previously identified as a liquid—liquid transition in the commodity polymers. 46,47 We believe that these transitions are associated with the relaxation of aggregates, as recently discussed by Sharma et al.⁴³ While this transition is observed across the set of polymers considered, its origin is not probed in detail here. Our focus rather is on the dominant secondary transitions observed in the polymers. There are clear transitions (T_{β}) in PTB7-TH and P(NDI2OD-T2) at -2and -21 °C, respectively. In PBnDT-FTAZ, there is a weak transition (T_{β}) at 20 °C followed by a stronger transition (T_{γ}) at -20 °C. In DPP4T, there is a strong transition (T_{β}) at 2 °C followed by a weaker transition (T_{ν}) at -25 °C. We attribute the dominant secondary transitions to be local relaxations, similar to recent reports. 43,48 The weaker transitions found in PBnDT-FTAZ (T_{β}) and DPP4T (T_{γ}) are likely associated with localized molecular relaxations along the backbone discussed further below. The multiple thermal transitions found in these polymers result in the dominant transition being labeled as T_{β} or T_{γ} . To simplify the discussion, we refer to the dominant thermal transition as $\{T_{\beta}\}$. We note that for the case of PBnDT-FTAZ, we have previously measured the polymer

relaxation with varying MW, showing that $\{T_{\beta}\}$ did not drop for the low MW samples supporting the argument that these are local relaxations. The COS_{RT} of each of these four polymers is quite large, ranging from 60 to 80% strain, as given in Table 1. The temperatures associated with a significant loss in toughness in P(NDI2OD-T2), PTB7-TH, PBnDT-FTAZ, and DPP4T were found to be -40, 0, -40, and -20 °C, respectively. The changes in crack features of the films at $T_{\rm b'}$ relative to RT are shown in Figure 3. PTB7-TH has $T_{b'}$ close to $\{T_{\beta}\}$, while PBnDT-FTAZ, DPP4T, and P(NDI2OD-T2) have a $T_{b'}$ that is between 14 and 26 °C below $\{T_{\beta}\}$. Based on these results, a straightforward conclusion is that the dominant secondary relaxations provide a significant source for ductility and toughness in CPs. To gain a more precise view of the role of the side-chain structure, backbone structure, and crystallinity on this behavior, we considered polymers with systematic structural variations next.

3.4. Role of Molecular Structure on Ductile-to-Brittle **Transition.** 3.4.1. Crystallinity. We first probe the role of crystallinity by comparing semicrystalline RR P3HT to amorphous regiorandom (RRa) P3HT. The DMA scan of RRa P3HT is given in Figure S13a, and a comparison of the $\tan \delta$ between RR P3HT and RRa P3HT is given Figure 4a. The thermal relaxations of RRa P3HT are found to be at 25 °C (T_{σ}) and -79 °C (T_{β}) , similar to that of RR P3HT. We also observe that $\{T_{\beta}\}$ was weaker and broader compared to that of RR P3HT. This observation is consistent with the report of Xie et al., which attributed the phenomenon to the weaker separation of an alkyl nanophase from the backbone.³⁸ The COS_{RT} of RRa P3HT is observed to be over 100%. To estimate the change in toughness, we strain the films to a similar extent of RR P3HT, namely, 80%. Similar to RR P3HT, there is no observed drop in toughness across the glass transition temperature. In addition, similar to RR P3HT, the RRa P3HT films lose toughness as the temperature drops below -30 °C. However, in RRa P3HT, the loss in ductility increases as the temperature drops, as can be observed from the evolution of cracks shown in Figures S8 and 4d. There is then a relatively abrupt change in crack features observed at -90 °C where large connected cracks across the film are observed. Thus, we identify -90 °C as $T_{b'}$ in RRa P3HT,

which is close to $\{T_{\beta}\}$ of -79 °C. The $T_{b'}$ in RRa P3HT is found to be at a higher temperature than RR P3HT, which had a $T_{b'}$ of -110 °C. The origin of this difference may be associated with improved molecular packing order in RR P3HT, allowing for chain slip below $\{T_{\beta}\}$.

3.4.2. Side-chain Structure. Next, we probe the role of sidechain structure by comparing PBnDT-FTAZ with PBoDT-FTAZ where the branched alkyl side-chains on the BDT unit were replaced with oligo(ethylene glycol) (OEG; $-(OC_2H_4)_3-OCH_3$), as shown in Figure 1. In the case of PBoDT-FTAZ, there were thermal transitions observed at 55 °C (T_{α}) , 21 °C (T_{β}) , and -39 °C $(T_{\gamma} \text{ or } \{T_{\beta}\})$, as shown in Figure 4b. The T_{α} of PBoDT-FTAZ was found to be significantly lower at 55 °C and more prominent than that of PBnDT-FTAZ. It is unclear if this transition continues to be associated with aggregates and we thus refer to it as T_{a^*} . The T_{β} of PBoDT-FTAZ was similar to that of PBnDT-FTAZ, while T_{ν} ($\{T_{\beta}\}$) was found to be roughly 13 °C lower. A drop in the relaxation temperature associated with the side-chains is expected in the case of OEG side-chains due to greater flexibility compared to the alkyl side-chains. 43,49 This provides support that $\{T_{\beta}\}$ in FTAZ-based polymers is associated with the side-chains. The change in the relaxation temperature related to changing the side-chains has been argued to be a plasticizing effect of the side-chain on the backbone.⁵⁰ As shown in Figures 4e and S9, the PBoDT-FTAZ films are found to have a large drop in toughness once below -40 °C that coincides with $\{T_{\beta}\}$. This contrasts with PBnDT-FTAZ, where $T_{b'}$ was approximately 14 °C below $\{T_{\beta}\}$. Similar to the case of P3HT, the difference between $T_{b'}$ and $\{T_{\beta}\}$ may be associated with the differences in the packing order in the film.

3.4.3. Backbone Structure. The impact of the backbone structure is probed in greater detail by comparing DPP4T with DPP-DTT, where the two thiophene units along the backbone in DPP4T are replaced with a thienothiophene unit. The DMA of DPP-DTT shows the α , β , and γ transitions at 129, 2, and -53 °C, as shown in Figure 4c. These are similar to the DPP4T relaxation temperatures also given in Figure 4c. The near identical $\{T_{\beta}\}$ supports the argument that this transition is associated with the polymer side-chains. It may also involve a relaxation of the backbone but would necessitate that it is a highly localized relaxation. As opposed to the similar thermal transitions of the DPP-based polymers, the room-temperature ductility of DPP-DTT is found to be significantly lower than DPP4T and the other donor-acceptor polymers considered that do not have clear T_g . The COS_{RT} of DPP-DTT is ~30%, as opposed to ~90% for DPP4T. The drop in ductility at room temperature is attributed to the increased backbone stiffness due to the fused thiophene rings in DPP-DTT.⁵¹ The stiffer backbone is confirmed when considering the polymer's persistence length, discussed below. The DPP-DTT films were found to lose significant ductility at -50 °C (Figure S10), which we define as $T_{b'}$. This loss in toughness is significantly below $\{T_{\beta}\}$ and closer to T_{γ} . While both DPP polymers show similar $\{T_{\beta}\}$, they have significantly different measured $T_{b'}$. We suspect that the lower COS_{RT} used to determine $T_{b'}$ in DPP-DTT plays a role in the large difference in the measured $T_{\rm h'}$. The T_{γ} observed at -50 °C may lead to some ductility that can support lower deformations. The impact of the T_{γ} relaxation would then be more apparent in the DPP-DTT films. The DPP-based polymers are also semicrystalline and crystal slip may also support plastic deformation to different extents and contribute to the observed behavior.

3.5. Thermal Relaxation Behavior. To look at the $\{T_{\beta}\}$ relaxation in more detail, we conducted DMA scans at different frequencies to create transition maps and determine the apparent activation energy of the transition. Here, we vary the frequency of applied strain from 0.1 to 10 Hz, with the results given in Figures 5a, S15, and S16. We find that all of the $\{T_{\beta}\}$

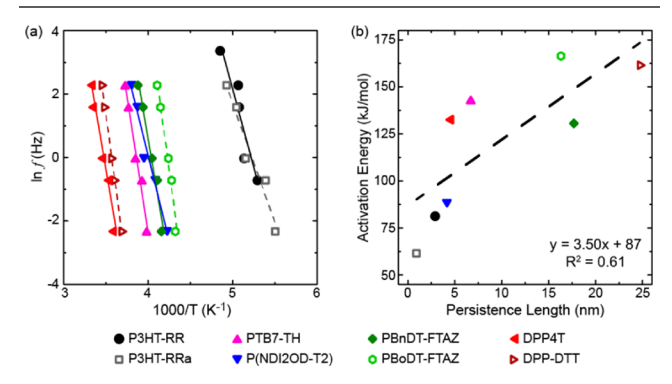


Figure 5. (a) Transition maps of the studied polymers at $\{T_{\beta}\}$ and (b) activation energy of $\{T_{\beta}\}$ transitions against persistence length of the polymers. The dotted line represents the linear fit of the scatter plot. Persistence lengths of RR P3HT and RRa P3HT were obtained from the work of McCulloch et al. ⁵⁵

transitions follow the Arrhenius behavior, characteristic of local relaxations, 52,53 although it should be noted that a larger frequency range should ideally be considered to support this argument. The activation energies determined from line fits to the data are given in Table S2 and found to be consistent with secondary relaxations found in other stiff polymers.^{52,54} It is worth comparing these to the apparent activation energies of the glass transitions in P3HT and PCDTBT, which were found to be 188 and 648 kJ/mol, respectively. The activation energy of the T_{σ} s is significantly higher than that found for the $\{T_{\beta}\}$ transitions. Given that the activation energy relates to the complexity of cooperative movement, this provides support that the $\{T_{\beta}\}$ transitions observed are localized in nature. While $\{T_{\beta}\}$ is a localized relaxation, it may involve both the side-chain and backbone. This is exemplified by considering the FTAZ-based polymers where we found that partially replacing the alkyl side-chains with OEG impacted multiple relaxations, suggesting coupling of the side-chain with other structural features of the polymer. Yet, in the DPP-based polymers, we found similar thermal transitions when replacing two thiophenes along the backbone with a fused thiophene moiety. These results suggest that the relaxation in the DPP polymers is highly localized. Recently, Xie et al. introduced a model that shows that varying the side-chains modifies the backbone relaxation temperature and argues that it is associated with the plasticizing effect of the side chains on the backbone. 50 However, the model was unable to predict relaxation temperatures observed for a number of polymers considered here. While it appears that $\{T_{\beta}\}$ is a local relaxation, the extent to which this relaxation is associated with the sidechains and backbone appears to be polymer dependent and requires further research to be specifically identified.

To explore the impact of backbone stiffness on the observed behavior, we determined the persistence length of the polymers. The persistence length (Table S2) was calculated with the approach introduced by Milner et al.,²³ as discussed in the SI. Looking at the systematic change in the backbone structure in the DPP-based polymers, we find that the COS_{RT}

drops significantly as the persistence length increases when going from DPP4T to DPP-DTT. Yet, we did not find a significant correlation between COS_{RT} and the stiffness of the polymer backbone when comparing all CPs considered. The ductility of the film depends on a number of factors including MW and entanglement density, among others. Thus, the backbone stiffness alone was not predictive of room-temperature ductility. We did find that there is a weak but statistically significant correlation between activation energy and persistence length in the polymers, as shown in Figure 5b. The activation energy is controlled by the energy of intermolecular interactions and chain rigidity. 19,53 The intermolecular interactions associated with the alkyl side-chains should be similar. Thus, the correlation observed supports the assertion that $\{T_{\beta}\}$ in the CPs does involve localized relaxation of the backbone. The local packing characteristics of the side-chains may also play a role in the activation energy. This is captured when comparing the activation energy of RRa P3HT ($E_a = 62$ kJ/mol) to RR P3HT ($E_a = 82 \text{ kJ/mol}$). The higher activation energy indicates a higher hindrance to molecular motion. Given the polymers have the same molecular structure, the difference in activation energy is attributed to differences in the packing order, stemming from greater persistence lengths in RR P3HT, and the less mobile chains extending from crystallites/aggregates. 38,55 The side-chains will also have different packing order that may include the formation of alkyl nanodomains in RR P3HT compared with less ordered side chains in RRa P3HT. 39 Finally, the difficulty in establishing a strong correlation between persistence length and activation energy may stem in part from the different extent of these interactions for a given polymer in a bulk solid relative to the simulations conducted in vacuo.

3.6. Discussion. Under tensile load, the polymer chains that are kinetically frozen (below T_g) in a coiled state begin to slide past one another while getting extended. As the polymer is cold drawn past yielding, the polymer chains get irreversibly extended as the segments of the chain undergo conformational changes before the polymer chain fails due to C-C bond rupture. 56-59 Extension of CP chains is expected to be due to conformal changes between ring structures that are connected through C-C bonds.⁵⁷ Enough free volume is required for these conformal changes to act along the polymer backbone, which exist due to molecular mobility active at temperatures below $T_{\rm g}$, e.g., local twisting/bending along the backbone, rotation of side-chains, etc. We propose that the $\{T_{\beta}\}$ transition in the CPs studied provides the necessary molecular mobility to allow for the movement of the polymer chains, resulting in ductile behavior when above $\{T_{\beta}\}$. A summary of $T_{b'}$ and $\{T_{\beta}\}$ for each polymer considered is provided in Figure 6, showing that they largely coincide with one another.

Importantly, most of the polymer films considered retain some ductility below $\{T_{\beta}\}$. This is evident in RR P3HT where the films strained at -110 °C show near continuous cracks at 80% strain, but when lowered to 60%, the cracks are small and pyramidal, showing an arrested nature (Figure S2). At 60% strain, the films have undergone plastic deformation prior to crack formation, which is not the behavior of a characteristically brittle material. This may be partially attributed to straining the film on an elastomer support, which is known to increase the fracture strain of the polymers films. This is clear when comparing COS_{RT} of the considered polymers and their rupture strain in FOW tests (Figure S17). Nevertheless, a brittle film will have a relatively low COS when on an

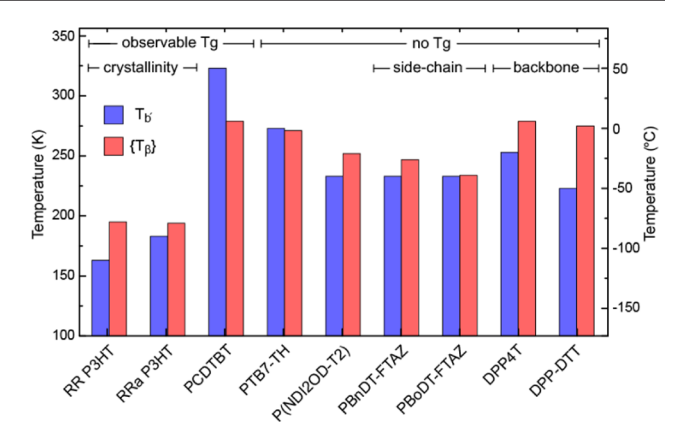


Figure 6. Summary of $T_{b'}$ and $\{T_{\beta}\}$ of the polymers studied.

elastomer, as observed for PMMA in Figure 2c. To understand this behavior, it is instructive to consider the crystal packing in conjugated polymer films after being strained. As the polymers are strained past their yield point, the long axis of the chains typically begins to preferentially orient in the direction of strain. 41,62 In highly strained donor-acceptor polymer films, the packing order of crystals has been shown to decrease. 41,63 The decreased order suggests that chain slip within the crystallites occurs upon deformation. Active slip systems have been previously investigated in RR P3HT, showing that slip along (100) and (010) planes is possible.²² This is likely to be the case in the other CPs considered as well. These slip systems may also be present in ordered aggregates of weakly crystalline conjugated polymers. For comparison, if we look at RRa P3HT and decrease the strain at $T_{b'}$ (Figure S8), we see reduced crack extension. However, the reduction in crack formation and propagation is not as large as observed with RR P3HT, suggesting that the films are less ductile at $T_{\rm b'}$. This is consistent with RRa P3HT being more disordered and having a lower density of active slip systems. The active slip systems likely allow for significant deformation below $\{T_{\beta}\}$ in contrast to the behavior observed in PMMA and brittle conjugated polymers such as PBTTT,⁶⁴ where the side-chain packing may prohibit these slip planes, resulting in channel cracks at low applied strains. In addition, the molecular mobility of the polymers may increase at the temperature that coincides with the onset of the drop in the storage modulus rather than the peak in $\tan \delta$. Thus, we also considered the crack behavior in PTB7-TH and PBnDT-FTAZ when strained at the temperature associated with the onset of the drop in the storage modulus, given in Figures S4 and S6. The PBnDT-FTAZ film continues to retain some ductility at this temperature, while the PTB7-TH films are found to have further embrittlement. The retention of the ductility in the PBnDT-FTAZ film supports the argument that active slip systems play a role in retaining ductility. The behavior of the PTB7-TH suggests that this is dependent on the polymer system and that further embrittlement can occur as the temperature is lowered beyond $T_{\mathbf{b}'}$.

These results have a number of implications for achieving mechanically robust polymer semiconductor devices. Foremost is the fact that a reduction in toughness is found to occur near $\{T_{\beta}\}$ in all conjugated polymers considered with the exception of PCDTBT. As a result, understanding the local relaxation behavior in the candidate conjugated polymers will assist in designing the tough active layer films. Furthermore, in the devices that employ blend films, understanding the impact of a

second molecule on the polymer's secondary relaxation will also be critical to ensure mechanically tough films. A second important finding is the ability of some polymer films to retain some ductility even below the secondary thermal relaxation. This is found in the case of RR P3HT where it has been established that the $\{T_{\beta}\}$ transition is associated with sidechain relaxations, as well as FTAZ-based polymers where the secondary relaxations appear to involve localized backbone relaxations. We propose that this is achieved through active slip systems in the ordered portion of the film. Exploring this mechanism in more detail may provide a route to achieve films with low viscoelastic relaxation at operating temperatures while retaining toughness and ductility. Reducing relaxation rates may limit morphological changes of the films purposely cast into a nonequilibrium state, which is the case in many highperformance organic solar cells.¹⁷ As a result, morphological burn-in degradation may be avoided.¹⁷

4. CONCLUSIONS

A suite of conjugated polymer semiconductors was studied to determine the role of thermomechanical relaxations on film toughness. The thermomechanical behavior was probed by dynamic mechanical analysis and the film toughness was probed by considering film ductility as a function of temperature. It was found that for most of the polymers considered, a large reduction in film toughness was found that corresponds to secondary thermal relaxations $\{T_B\}$. The secondary nature, i.e., local nonsegmental motion, of these thermal relaxations was probed through frequency maps in the DMA and by comparing the polymers with systematic variation to the side-chain and backbone structure. It was found that while the loss in toughness is clearly associated with $\{T_{\rm b}\}$, the differences in the molecular structure and packing behavior influence the relative changes in ductility. Furthermore, we observed that a number of polymers retain some ductility below their dominant secondary thermal relaxation temperature. While the origin of this behavior requires further exploration, we propose that crystallites/aggregates in the films allow for energy dissipation through chain slip. It is clear that secondary relaxation behavior driven in part by side-chain characteristics is critical to CP film toughness. Through this observation, the design of the side-chain structures may be used to not only improve the solubility and promote the packing order but also improve the thermal and mechanical stability.

ASSOCIATED CONTENT

Supporting Information

The Supporting Information is available free of charge at https://pubs.acs.org/doi/10.1021/acs.chemmater.0c01910.

Recipes of film processing, optical microscope images of the films at various strains and temperatures, DMA plots of the polymers, film on water measurements, DSC plots of the polymers, and density function theory calculations (PDF)

AUTHOR INFORMATION

Corresponding Author

Brendan T. O'Connor – Department of Mechanical and Aerospace Engineering, and Organic and Carbon Electronics Laboratories (ORaCEL), North Carolina State University, Raleigh, North Carolina 27695, United States; orcid.org/0000-0002-8999-5184; Email: btoconno@ncsu.edu

Authors

Nrup Balar – Department of Mechanical and Aerospace Engineering, and Organic and Carbon Electronics Laboratories (ORaCEL), North Carolina State University, Raleigh, North Carolina 27695, United States; ◎ orcid.org/0000-0003-3243-3583

Salma Siddika — Department of Materials Science and Engineering, and Organic and Carbon Electronics Laboratories (ORaCEL), North Carolina State University, Raleigh, North Carolina 27695, United States

Somayeh Kashani — Department of Physics, and Organic and Carbon Electronics Laboratories (ORaCEL), North Carolina State University, Raleigh, North Carolina 27695, United States

Zhengxing Peng – Department of Physics, and Organic and Carbon Electronics Laboratories (ORaCEL), North Carolina State University, Raleigh, North Carolina 27695, United States

Jeromy James Rech — Department of Chemistry, University of North Carolina, Chapel Hill, North Carolina 27599, United States; ⊚ orcid.org/0000-0001-7963-9357

Long Ye – School of Materials Science and Engineering, Tianjin University, Tianjin 300072, P. R. China

Wei You − Department of Chemistry, University of North Carolina, Chapel Hill, North Carolina 27599, United States; orcid.org/0000-0003-0354-1948

Harald Ade – Department of Physics, and Organic and Carbon Electronics Laboratories (ORaCEL), North Carolina State University, Raleigh, North Carolina 27695, United States

Complete contact information is available at: https://pubs.acs.org/10.1021/acs.chemmater.0c01910

Notes

The authors declare no competing financial interest.

■ ACKNOWLEDGMENTS

The authors gratefully acknowledge support for this research through NSF CAREER award 1554322 and NSF award 1639429. The authors would also like to thank Dr. X. Zhao (Changchun Institute of Applied Chemistry, Chinese Academy of Sciences) for help with the HT-GPC measurement.

ABBREVIATIONS

PMMA	poly(methyl methacrylate)
PSS	poly(4-styrenesulfonic acid)
P3HT	poly(3-hexylthiphene)
PCDTBT	poly[N-9'-heptadecanyl-2,7-carbazole-alt-
	5,5-(4',7'-di-2-thienyl-2',1',3'-benzothiadia- zole)]
PTB7-TH	poly[4,8-bis(5-(2-ethylhexyl)thiophen-2-yl)-
	benzo[1,2- <i>b</i> ;4,5- <i>b</i> ']dithiophene-2,6-diyl- <i>alt</i> -
	(4-(2-ethylhexyl)-3-fluorothieno[3,4-b]-
	thiophene-)-2-carboxylate-2-6-diyl)]
P(NDI2OD-T2)	$poly\{[N,N'-bis(2-octyldodecyl)-$
	naphthalene-1,4,5,8-bis(dicarboximide)-2,6-
	$diyl$]- alt -5,5'-(2,2'-bithiophene)}
PBnDT-FTAZ	poly[4-(5-(4,8-bis(3-butylnonyl)benzo[1,2-
	b:4,5-b'] dithiophen-2-yl) thiophen-2-yl)-2-
	(2-butyloctyl)-5,6-difluoro-7-(thiophen-2-
	yl)- $2H$ -benzo[d][$1,2,3$]triazole]

PBoDT-FTAZ poly[4-(5-(4,8-bis(2-(2-(2-methoxyethoxy)-

ethoxy)ethoxy)benzo[1,2-b:4,5-b']-dithiophen-2-yl)thiophen-2-yl)-2-(2-buty-loctyl)-5,6-difluoro-7-(thiophen-2-yl)-2H-

benzo[d][1,2,3]triazole]

DPP4T poly[2,5-bis(2-octyldodecyl) pyrrolo[3,4-c]

pyrrole-1,4-(2*H*,5*H*)-dione-3,6-diyl-*alt*-(2,2';5',2";5",2""-quaterthiophen-5,5"'-

diyl)]

DPP-DTT poly[2,5-(2-octyldodecyl)-3,6-diketopyrro-

lopyrrole-alt-5,5-(2,5-di(thien-2-yl)thieno

[3,2-b]thiophene)

REFERENCES

- (1) Xu, J.; Wang, S.; Wang, G.-J. N.; Zhu, C.; Luo, S.; Jin, L.; Gu, X.; Chen, S.; Feig, V. R.; To, J. W. F.; Rondeau-Gagne', S.; Park, J.; Schroeder, B. C.; Lu, C.; Oh, J.; Wang, Y.; Kim, Y.; Yan, H.; Sinclair, R.; Zhou, D.; Xue, G.; Murmann, B.; Linder, C.; Cai, W.; Tok, J. B. H.; Chung, J.; Bao, Z. Highly Stretchable Polymer Semiconductor Films through the Nanoconfinement Effect. *Science* **2017**, *355*, 59–64.
- (2) Schwartz, G.; Tee, B. C.-K.; Mei, J.; Appleton, A. L.; Kim, D. H.; Wang, H.; Bao, Z. Flexible Polymer Transistors with High Pressure Sensitivity for Application in Electronic Skin and Health Monitoring. *Nat. Commun.* **2013**, *4*, No. 1859.
- (3) White, M. S.; Kaltenbrunner, M.; Głowacki, E. D.; Gutnichenko, K.; Kettlgruber, G.; Graz, I.; Aazou, S.; Ulbricht, C.; Egbe, D. A. M.; Miron, M. C.; Major, Z.; Scharber, M. C.; Sekitani, T.; Someya, T.; Bauer, S.; Saricifti, N. S. Ultrathin, Highly Flexible and Stretchable PLEDs. *Nat. Photonics* **2013**, *7*, 811–816.
- (4) Yu, Z.; Niu, X.; Liu, Z.; Pei, Q. Intrinsically Stretchable Polymer Light-Emitting Devices Using Carbon Nanotube-Polymer Composite Electrodes. *Adv. Mater.* **2011**, *23*, 3989–3994.
- (5) Krebs, F. C.; Espinosa, N.; Hösel, M.; Søndergaard, R. R.; Jørgensen, M. 25th Anniversary Article: Rise to Power-OPV-Based Solar Parks. *Adv. Mater.* **2014**, *26*, 29–39.
- (6) Kaltenbrunner, M.; White, M. S.; Głowacki, E. D.; Sekitani, T.; Someya, T.; Sariciftci, N. S.; Bauer, S. Ultrathin and Lightweight Organic Solar Cells with High Flexibility. *Nat. Commun.* **2012**, 3, No. 770.
- (7) Sekitani, T.; Yokota, T.; Zschieschang, U.; Klauk, H.; Bauer, S.; Takeuchi, K.; Takamiya, M.; Sakurai, T.; Someya, T. Organic Nonvolatile Memory Transistors for Flexible Sensor Arrays. *Science* **2009**, *326*, 1516–1519.
- (8) Yi, H. T.; Payne, M. M.; Anthony, J. E.; Podzorov, V. Ultra-Flexible Solution-Processed Organic Field-Effect Transistors. *Nat. Commun.* **2012**, *3*, No. 1259.
- (9) Sen, P.; Yang, R.; Rech, J. J.; Feng, Y.; Ho, C. H. Y.; Huang, J.; So, F.; Kline, R. J.; You, W.; Kudenov, M. W.; O'Connor, B. T. Panchromatic All-Polymer Photodetector with Tunable Polarization Sensitivity. *Adv. Opt. Mater.* **2019**, *7*, No. 1801346.
- (10) Wu, S. Secondary Relaxation, Brittle-ductile Transition Temperature, and Chain Structure. *J. Appl. Polym. Sci.* **1992**, *46*, 619–624.
- (11) O'Connor, T. F.; Zaretski, A. V.; Shiravi, B. A.; Savagatrup, S.; Printz, A. D.; Diaz, M. I.; Lipomi, D. J. Stretching and Conformal Bonding of Organic Solar Cells to Hemispherical Surfaces. *Energy Environ. Sci.* **2014**, *7*, 370–378.
- (12) Li, Y.; Tatum, W. K.; Onorato, J. W.; Zhang, Y.; Luscombe, C. K. Low Elastic Modulus and High Charge Mobility of Low-Crystallinity Indacenodithiophene-Based Semiconducting Polymers for Potential Applications in Stretchable Electronics. *Macromolecules* **2018**, *51*, 6352–6358.
- (13) Li, Y.; Tatum, W. K.; Onorato, J. W.; Barajas, S. D.; Yang, Y. Y.; Luscombe, C. K. An Indacenodithiophene-Based Semiconducting Polymer with High Ductility for Stretchable Organic Electronics. *Polym. Chem.* **2017**, *8*, 5185–5193.

- (14) Müller, C. On the Glass Transition of Polymer Semiconductors and Its Impact on Polymer Solar Cell Stability. *Chem. Mater.* **2015**, 27, 2740–2754.
- (15) Chen, S. A.; Ni, J. M. Structure/Properties of Conjugated Conductive Polymers. 1. Neutral Poly(3-Alkythiophene)S. *Macromolecules* **1992**, *25*, 6081–6089.
- (16) de Zerio, A. D.; Müller, C. Glass Forming Acceptor Alloys for Highly Efficient and Thermally Stable Ternary Organic Solar Cells. *Adv. Energy Mater.* **2018**, No. 1702741.
- (17) Ghasemi, M.; Hu, H.; Peng, Z.; Rech, J. J.; Angunawela, I.; Carpenter, J. H.; Stuard, S. J.; Wadsworth, A.; McCulloch, I.; You, W.; Ade, H. Delineation of Thermodynamic and Kinetic Factors That Control Stability in Non-Fullerene Organic Solar Cells. *Joule* **2019**, *3*, 1328–1348.
- (18) Kambour, R. P.; Robertson, R. E. Polymer Science: A Materials Science Handbook; Jenkins, A. D., Eds.; Elsevier: Amsterdam, 1972.
- (19) Yee, A. F.; Smith, S. A. Molecular Structure Effects on the Dynamic Mechanical Spectra of Polycarbonates. *Macromolecules* 1981, 14, 54–64.
- (20) Boyer, R. F. Dependence of Mechanical Properties on Molecular Motion in Polymers. *Polym. Eng. Sci.* **1968**, *8*, 161–185.
- (21) Jho, J. Y.; Yee, A. F. Secondary Relaxation Motion in Bisphenol A Polycarbonate. *Macromolecules* **1991**, *24*, 1905–1913.
- (22) Zhao, B.; Awartani, O.; O'Connor, B.; Zikry, M. A. A Direct Correlation of X-Ray Diffraction Orientation Distributions to the in-Plane Stiffness of Semi-Crystalline Organic Semiconducting Films. *Appl. Phys. Lett.* **2016**, *108*, No. 181902.
- (23) Zhang, W.; Gomez, E. D.; Milner, S. T. Predicting Chain Dimensions of Semiflexible Polymers from Dihedral Potentials. *Macromolecules* **2014**, 47, 6453–6461.
- (24) Balar, N.; Rech, J. J.; Henry, R.; Ye, L.; Ade, H.; You, W.; O'Connor, B. T. The Importance of Entanglements in Optimizing the Mechanical and Electrical Performance of All-Polymer Solar Cells. *Chem. Mater.* **2019**, *31*, 5124–5132.
- (25) Price, S. C.; Stuart, A. C.; Yang, L.; Zhou, H.; You, W. Fluorine Substituted Conjugated Polymer of Medium Band Gap Yields 7% Efficiency in Polymer—Fullerene Solar Cells. *J. Am. Chem. Soc.* **2011**, 133, 4625–4631.
- (26) Chen, Z.; Yan, L.; Rech, J. J.; Hu, J.; Zhang, Q.; You, W. Green-Solvent-Processed Conjugated Polymers for Organic Solar Cells: The Impact of Oligoethylene Glycol Side Chains. *ACS Appl. Polym. Mater* **2019**, *1*, 804–814.
- (27) Sharma, A.; Pan, X.; Campbell, J. A.; Andersson, M. R.; Lewis, D. A. Unravelling the Thermomechanical Properties of Bulk Heterojunction Blends in Polymer Solar Cells. *Macromolecules* **2017**, 50, 3347–3354.
- (28) Song, R.; Schrickx, H.; Balar, N.; Siddika, S.; Sheikh, N.; O'Connor, B. T. Unveiling the Stress-Strain Behavior of Conjugated Polymer Thin Films for Stretchable Device Applications. *Macromolecules* **2020**, *53*, 1988–1997.
- (29) Crowe-Willoughby, J. A.; Weiger, K. L.; Ozcam, A. E.; Genzer, J. Formation of Silicone Elastomer Networks Films with Gradients in Modulus. *Polymer* **2010**, *51*, 763–773.
- (30) Porter, C. E.; Blum, F. D. Thermal Characterization of PMMA Thin Films Using Modulated Differential Scanning Calorimetry. *Macromolecules* **2000**, *33*, 7016–7020.
- (31) Geng, K.; Tsui, O. K. C. Effects of Polymer Tacticity and Molecular Weight on the Glass Transition Temperature of Poly-(Methyl Methacrylate) Films on Silica. *Macromolecules* **2016**, *49*, 2671–2678.
- (32) Bay, R. K.; Crosby, A. J. Uniaxial Extension of Ultrathin Freestanding Polymer Films. ACS Macro Lett. 2019, 8, 1080–1085.
- (33) Kim, J.-H.; Nizami, A.; Hwangbo, Y.; Jang, B.; Lee, H.-J.; Woo, C.-S.; Hyun, S.; Kim, T.-S. Tensile Testing of Ultra-Thin Films on Water Surface. *Nat. Commun.* **2013**, *4*, No. 3283.
- (34) Balar, N.; O'Connor, B. T. Correlating Crack Onset Strain and Cohesive Fracture Energy in Polymer Semiconductor Films. *Macromolecules* **2017**, *50*, 8611–8618.

- (35) Alkhadra, M. A.; Root, S. E.; Hilby, K. M.; Rodriquez, D.; Sugiyama, F.; Lipomi, D. J. Quantifying the Fracture Behavior of Brittle and Ductile Thin Films of Semiconducting Polymers. *Chem. Mater* **2017**, *29*, 10139–10149.
- (36) Rahbar, N.; Wolf, K.; Orana, A.; Fennimore, R.; Zong, Z.; Meng, J.; Papandreou, G.; Maryanoff, C.; Soboyejo, W. Adhesion and Interfacial Fracture Toughness between Hard and Soft Materials. *J. Appl. Phys.* **2008**, *104*, No. 103533.
- (37) Carswell, T. S.; Nason, J. K. In Effect of Environmental Conditions on the Mechanical Properties of Organic Plastics; Symposium on Plastics, Philadelphia District Meeting; American Society for Testing Materials: Philadephia, 1944.
- (38) Xie, R.; Lee, Y.; Aplan, M. P.; Caggiano, N. J.; Müller, C.; Colby, R. H.; Gomez, E. D. Glass Transition Temperature of Conjugated Polymers by Oscillatory Shear Rheometry. *Macromolecules* **2017**, *50*, 5146–5154.
- (39) Pankaj, S.; Hempel, E.; Beiner, M. Side-Chain Dynamics and Crystallization in a Series of Regiorandom Poly(3-Alkylthiophenes). *Macromolecules* **2009**, 42, 716–724.
- (40) Lu, X.; Hlaing, H.; Germack, D. S.; Peet, J.; Jo, W. H.; Andrienko, D.; Kremer, K.; Ocko, B. M. Bilayer Order in a Polycarbazole-Conjugated Polymer. *Nat. Commun.* **2012**, 3, No. 795.
- (41) Sun, T.; Song, R.; Balar, N.; Sen, P.; Kline, R. J.; O'Connor, B. T. Impact of Substrate Characteristics on Stretchable Polymer Semiconductor Behavior. ACS Appl. Mater. Interfaces 2019, 11, 3280–3289.
- (42) Balar, N.; Xiong, Y.; Ye, L.; Li, S.; Nevola, D.; Dougherty, D. B.; Hou, J.; Ade, H.; O'Connor, B. T. Role of Polymer Segregation on the Mechanical Behavior of All-Polymer Solar Cell Active Layers. *ACS Appl. Mater. Interfaces* **2017**, *9*, 43886–43892.
- (43) Sharma, A.; Pan, X.; Bjuggren, J. M.; Gedefaw, D.; Xu, X.; Kroon, R.; Wang, E.; Campbell, J. A.; Lewis, D. A.; Andersson, M. R. Probing the Relationship between Molecular Structures, Thermal Transitions, and Morphology in Polymer Semiconductors Using a Woven Glass-Mesh-Based DMTA Technique. *Chem. Mater.* **2019**, *31*, No. 6740.
- (44) Snyder, C. R.; DeLongchamp, D. M. Glassy Phases in Organic Semiconductors. *Curr. Opin. Solid State Mater. Sci.* **2018**, 22, 41–48.
- (45) Yao, H.; Ye, L.; Zhang, H.; Li, S.; Zhang, S.; Hou, J. Molecular Design of Benzodithiophene-Based Organic Photovoltaic Materials. *Chem. Rev.* **2016**, *116*, 7397–7457.
- (46) Lobanov, A. M.; Frenkel', S. Y. The Nature of the So-Called "Liquid-Liquid" Transition in Polymer Melts. A Review. *Polym. Sci. U.S.S.R.* 1980, 22, 1150–1163.
- (47) Stadnicki, S. J.; Gillham, J. K.; Boyer, R. F. The Tll (>T_g) Transition of Atactic Polystyrene. *J. Appl. Polym. Sci.* **1976**, 20, 1245–1275.
- (48) Schroeder, B. C.; Chiu, Y.-C.; Gu, X.; Zhou, Y.; Xu, J.; Lopez, J.; Lu, C.; Toney, M. F.; Bao, Z. Non-Conjugated Flexible Linkers in Semiconducting Polymers: A Pathway to Improved Processability without Compromising Device Performance. *Adv. Electron. Mater.* **2016**, *2*, No. 1600104.
- (49) Sugiyama, F.; Kleinschmidt, A. T.; Kayser, L. V.; Rodriquez, D.; Finn, M.; Alkhadra, M. A.; Wan, J. M.-H.; Ramírez, J.; Chiang, A. S.-C.; Root, S. E.; Savagatrup, S.; Lipomi, D. J. Effects of Flexibility and Branching of Side Chains on the Mechanical Properties of Low-Bandgap Conjugated Polymers. *Polym. Chem.* **2018**, *9*, 4354–4363.
- (50) Xie, R.; Weisen, A. R.; Lee, Y.; Aplan, M. A.; Fenton, A. M.; Masucci, A. E.; Kempe, F.; Sommer, M.; Pester, C. W.; Colby, R. H.; Gomez, E. D. Glass Transition Temperature from the Chemical Structure of Conjugated Polymers. *Nat. Commun.* **2020**, *11*, No. 893.
- (51) Roth, B.; Savagatrup, S.; De Los Santos, N. V.; Hagemann, O.; Carle, J. E.; Helgesen, M.; Livi, F.; Bundgaard, E.; Søndergaard, R. R.; Krebs, F. C.; Lipomi, D. J. Mechanical Properties of a Library of Low-Bandgap Polymers. *Chem. Mater.* **2016**, *28*, 2363–2373.
- (52) Bershtein, V. A.; Egorov, V. M.; Egorova, L. M.; Ryzhov, V. A. The Role of Thermal Analysis in Revealing the Common Molecular Nature of Transitions in Polymers. *Thermochim. Acta* **1994**, 238, 41–73.

- (53) Matsuoka, S. Relaxation Phenomena in Polymers; Hanser Publishers: Cincinnati, OH, 1992.
- (54) Johari, G. P.; Goldstein, M. Viscous Liquids and the Glass Transition. II. Secondary Relaxations in Glasses of Rigid Molecules. *J. Chem. Phys.* **1970**, *53*, 2372–2388.
- (55) McCulloch, B.; Ho, V.; Hoarfrost, M.; Stanley, C.; Do, C.; Heller, W. T.; Segalman, R. A. Polymer Chain Shape of Poly(3-Alkylthiophenes) in Solution Using Small-Angle Neutron Scattering. *Macromolecules* **2013**, *46*, 1899–1907.
- (56) Wu, S. Chain Structure, Phase Morphology, and Toughness Relationships in Polymers and Blends. *Polym. Eng. Sci.* **1990**, *30*, 753–761.
- (57) Vezie, M. S.; Few, S.; Meager, I.; Pieridou, G.; Dörling, B.; Ashraf, R. S.; Goñi, A. R.; Bronstein, H.; McCulloch, I.; Hayes, S. C.; Campoy-Quiles, M.; Nelson, J. Exploring the Origin of High Optical Absorption in Conjugated Polymers. *Nat. Mater.* **2016**, *15*, 746–753.
- (58) Hutchinson, I.; Ward, I.; Willis, H.; Zichy, V. Infra-Red Measurements on One-Way Drawn Poly(Ethylene Terephthalalate) Films Subjected to Constant Strain. *Polymer* **1980**, *21*, 55–65.
- (59) Aharoni, S. M. Correlations between Chain Parameters and Failure Characteristics of Polymers below Their Glass Transition Temperature. *Macromolecules* **1985**, *18*, 2624–2630.
- (60) Frisch, H. L.; Stern, S. A. Diffusion of Small Molecules in Polymers. Crit. Rev. Solid State Mater. Sci. 1983, 11, 123–187.
- (61) Menard, K. P. Dynamic Mechanical Analysis: A Practical Introduction; CRC Press: Boca Raton, FL, 1999.
- (62) O'Connor, B.; Kline, R. J.; Conrad, B. R.; Richter, L. J.; Gundlach, D.; Toney, M. F.; DeLongchamp, D. M. Anisotropic Structure and Charge Transport in Highly Strain-Aligned Regioregular Poly(3-hexylthiophene). *Adv. Funct. Mater.* **2011**, *21*, 3697–3705
- (63) Scott, J. I.; Xue, X.; Wang, M.; Kline, R. J. J.; Hoffman, B. C.; Dougherty, D.; Zhou, C.; Bazan, G.; O'Connor, B. T. Significantly Increasing the Ductility of High Performance Polymer Semiconductors through Polymer Blending. *ACS Appl. Mater. Interfaces* **2016**, *8*, 14037–14045.
- (64) O'Connor, B.; Chan, E. P.; Chan, C.; Conrad, B. R.; Richter, L. J.; Kline, R. J.; Heeney, M.; McCulloch, I.; Soles, C. L.; DeLongchamp, D. M. Correlations between Mechanical and Electrical Properties of Polythiophenes. *ACS Nano* **2010**, *4*, 7538–7544.